Decision-making components and times revealed by the single-trial electro-encephalogram

Gabriel Weindel[1,2*§], **Jelmer P. Borst**[1†], **Leendert van Maanen**[2†]

[1]University of Groningen, The Netherlands; [2]Utrecht University, The Netherlands

***For correspondence:** gabriel.weindel@unil.ch (GW)

[†]These authors contributed equally to this work

Present address: [§]Institut de Psychologie, Université de Lausanne, Switzerland

Abstract Decision-making stems from a sequence of information processing steps between the choice onset and the response. Despite extensive research, uncertainty remains about the actual cognitive sequence involved in the reaction time. Using the hidden multivariate pattern method we modeled the single-trial electroencephalogram of participants performing a decision task as a sequence of an unknown number of events estimated as trial-recurrent, time-varying, stable topographies. We provide evidence for three events occurring during participant's decision making, respectively representing encoding, attention orientation, and decision. This interpretation is supported by the observation that a targeted manipulation of stimulus intensity yields Piéron's law in the interval between encoding and attention orientation, and Fechner's law in the interval between attention orientation and decision. This final, decision-related, event is represented in the brain as a positive burst in parietal areas whose timing, amplitude and build-up predict the participants' decision accuracy.

Introduction

Making a decision involves several information processing steps within the time from the presentation of a stimulus to the response. The sum of the times required for the completion of each of these precessing steps is the reaction time (RT). Specific processes differ between experimental paradigms, but a minimal set that seems to be agreed upon involves encoding of the choice elements, followed by weighting the evidence for each choice, and initiating a response (***Donders, 1868***; ***Ratcliff and McKoon, 2008***; ***Zylberberg et al., 2011***; ***Luce, 1986***). Despite being an almost two century old problem (***von Helmholtz, 2021***) it is unclear how the RT emerges from these putative components.

The answer to this problem has first been hampered by the relatively poor information gained from RT and response-accuracy data alone. Co-registering physiological signals can clarify and extend conclusions about information processing steps in the RT (***Turner et al., 2017***). Evidence for the putative components that make up RT has been found by registering the electro-encephalogram (EEG) during decision tasks. First, a negative deflection in occipital electrodes happening around 200ms after the presentation of a choice, the N200, has been associated with visual encoding of the choice elements by participants (***Nunez et al., 2019***; ***Ritter et al., 1979***). Second, EEG data has shown that the weighting of evidence towards the alternatives is associated with a positive voltage developing over centro-parietal electrodes after early visual potentials (***Kutas et al., 1977***). Computational models of decision-making explain the experimental effects observed on these centro-parietal components as an evidence accumulation mechanism (***O'Connell et al., 2012***; ***Kelly et al., 2021***). Lastly, a component preceding the response has been shown to lateralize with the side of

the executed response (***Coles et al., 1985***). This lateralized readiness potential has later been described as arising from an accumulation-to-bound mechanism describing the decision to produce a movement (***Schurger et al., 2012***).

However, the knowledge gained on the nature and latencies of cognitive processes within the RT from such electrophysiological components is limited by the low signal-to-noise ratio of classical neural measurements. To improve the SNR, researchers usually rely on information derived from the averaging of these signals over many trials. Unfortunately, averaging time-varying signals will result in an average waveform that misrepresents the underlying single-trial events (***Luck, 2005***; ***Borst and Anderson, 2024***). In the case of decision-making, several studies have shown wide by-trial variation of the timing of cognitively relevant neural events (***Vidaurre et al., 2019***; ***Smyrnis et al., 2012***; ***Weindel et al., 2021***; ***Weindel, 2021***). Furthermore, averaged components are further distorted by the fact that multiple cognitive processes and associated EEG components are typically present within trials and overlap in time between trials (***Woldorff, 1993***), forcing researchers to study physiological components in isolation. Overall this leaves the possibility open that the single-trial physiological events might not resemble their trial-aggregated counterparts.

In intracranial recordings, it has been suggested that neuronal activity in the lateral intra-parietal area of macaques performing a decision task was better explained by step-like functions with time-varying onsets at the trial-level rather than a ramping activity mimicking evidence accumulation as suggested by the averaging of these traces (***Latimer et al., 2015***). In human EEG data, a similar interpretation has been offered in which the classical observation of a slowly evolving centro-parietal positivity, scaling with evidence accumulation, was suggested to result from the overlap of time-varying response-related activity (***Frömer et al., 2024***). Although debated (***Steinemann et al., 2024***; ***Shadlen et al., 2016***; ***O'Connell et al., 2024***), these results shed doubts on the typical interpretation of neural correlates of cognitive processes involved in decision-making. As, to date, no study has been able to provide single-trial evidence of multiple EEG components involved in decision-making, the steps within the RT and their location both in time and in the brain remain unknown.

One potential solution mixing both behavior and multivariate analysis of single-trial neural signal has emerged through the development of the hidden multivariate methods (***Weindel et al., 2024***; ***Anderson et al., 2016***). These methods model the neural data of each trial as a sequence of short-lived multivariate cortex-wide events, repeated at each trial, whose timing varies on a trial-basis and define the RT. In the case of EEG, it is assumed that any cognitive step involved in the RT is represented by a specific topography recurring across trials. The time-jitter in the topography is accounted by estimating, for each of these events, a by-trial distribution where the expected time of the peak of the topography is given by the time distribution of the previous event's peak and the expected time distribution of the current event. By constraining, through the recorded behavior, the search for trial-shared sequential activations in the EEG during estimated ranges of time, the hidden multivariate pattern (HMP) model (***Weindel et al., 2024***) provides an estimation on the number of events and their single-trial location during each trial. Previous similar approaches have shown that different information processing steps can be extracted from the EEG in a wide range of tasks (***Berberyan et al., 2021***; ***Zhang et al., 2018***; ***Anderson et al., 2016***, ***2018***; ***Krause et al., 2024***). Building on previous work (***Van Maanen et al., 2021***), we expect that the EEG data of a decision-making task will be decomposed into task relevant intervals indexing the information processing steps in the RT. In the current study we combine this single-trial modeling strategy with strong theoretical expectations regarding the impact of experimental manipulations on the latent information processing steps during decision-making.

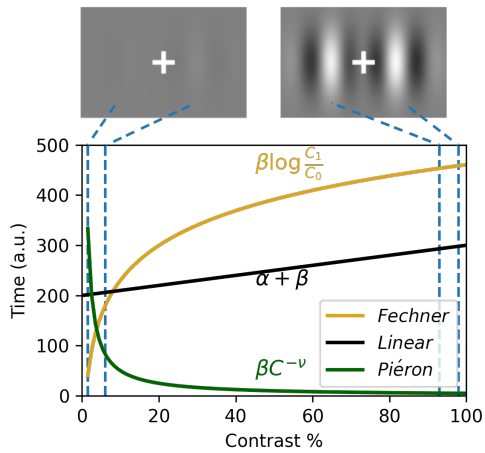

Figure 1. Contrast manipulation used in the experiment
Top shows two example stimuli illustrating minimum (left) and maximum (right) contrast values. Bottom panel shows the prediction for the Piéron, the Fechner and the linear laws for all contrast levels (C) used in the study for a fixed set of parameters. α, β and ν are respectively the estimated participant specific intercept, slope and exponent for the three laws. The Fechner diffusion law additionally includes non-decision and decision threshold parameters (see methods).

The task of the participants was to answer which of two sinusoidal gratings flanking a fixation cross displayed the highest contrast (***Figure 1***A). We hypothesize that different cognitive processes are associated with two of the oldest laws in psychophysics: Piéron's law (***Piéron, 1913***) and Fechner's law (***Fechner, 1860***). In order to elucidate these laws we manipulated the contrast of both gratings while keeping their difference constant (see the two example trials in ***Figure 1***, one with an average contrast of 5%, and one with an average contrast of 95%, both with a difference of 5%).

The manipulation of contrast has two opposing predictions on the cognitive processes involved in decision-making: the time to perceive the two stimuli (and thus the choice situation) should follow a negative power law with the stimulus intensity according to Piéron's law (***Figure 1***, green curve). In contradistinction, Fechner's law states that the perceived difference between the two patches follows the logarithm of the physical difference of contrast of the two patches (***Figure 1***, yellow curve). As the task of our participant is to judge the contrast difference, Fechner's law should implement decision difficulty. Given this we connected this law to the classical diffusion decision models by replacing the rate of accumulation with Fechner's law, as done for other mathematical functions (***Palmer et al., 2005***). This coupling with an evidence accumulation model further allows to connects the RT to the proportion of correct responses. Thus we expect that, at least the time needed for participants to perceive the stimulus and the time needed to decide upon the stimulus should have opposite relations with the contrast levels. To test the generalizability of our findings and allow comparison to standard decision-making tasks, we also included a speed-accuracy manipulation by asking participants to either focus on the speed or the accuracy of their responses in different experimental blocks.

Results

All results were obtained from the data of the 26 participants, with the recorded EEG band-passed filtered between 0.01 and 40Hz. Trials with RT lower than 100 ms or higher than 3000 ms or in which an electrode exceeded a rejection threshold of 100 μV during the RT were rejected (3.1% of trials were rejected, see Method section for a full report). The hidden multivariate pattern model implemented assumed that a task-related multivariate pattern event is represented by a 50ms wide half-sine and whose timing varies from trial to trial based on a gamma distribution with a shape parameter of 2 and a scale free-to-vary per event (***Weindel et al., 2024***).

Perceptual and decision effects compete at the behavioral level

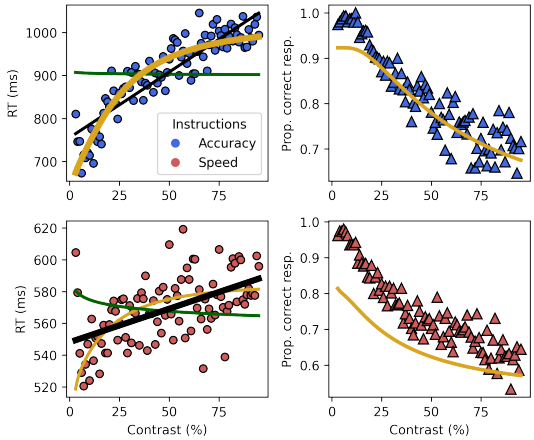

Figure 2. behavioral results partially support Fechner's law
Left: Mean RT (dot) and average fit (line) over trials and participants for each contrast level used in the study with Accuracy (Top) and Speed (Bottom) instructions. Right: Mean proportion of correct responses averaged over trials and participant for each contrast level (triangles) along the average predicted proportions for the Fechner diffusion models (line) in Accuracy (Top) and Speed (Bottom).

Figure 2 shows the mean RT and proportion of correct responses. To test what law best described the RT data we fitted the two opposing psychological laws and an atheoretical linear model. Using a leave-one-out cross-validation strategy we observed that the best fitting model is the Fechner diffusion model in the accuracy condition and the linear model in the speed focused condition (***Table 1***). Having fitted the Fechner law in a diffusion model framework on the RT we can use the estimated parameters to predict the proportion of correct responses. Despite only estimating parameters on the RT, the prediction of the model is relatively close to the observed proportion of correct responses (R^2 = 0.84) in the accuracy condition but the predictive power is very low when speed is emphasized (R^2 = 0.03).

The behavioral results thus tell two stories: first, as long as accuracy was stressed, Fechner's law predicted the RTs and predicted the proportion of correct responses closely. However, when speed was stressed – and consequently one or more of the underlying cognitive processes was shorter – Fechner's law did no longer explain the behavioral data, instead a linear model fitted the data best. It is unlikely that neither Piéron nor Fechner law impact the RT in the speed condition, instead this result is likely due to the composite nature of the RT. We explored this in the next sections by applying HMP to the EEG data.

Three trial-recurrent sequential events occur in the EEG during decisions

modeling the EEG between stimulus and response as a sequence of events with varying by-trial latencies revealed that three events are necessary to account for the EEG data. ***Figure 3*** shows the estimated model components with the inter-event time distributions and the weights of each detected event in the electrode space. The cumulative probability of occurrences of the events displayed in ***Figure 3*** show how variable the latency of the events was over trials. Overlaid on the probabilities we represent each event at their averaged time location as well as the averaged electrode activity. These topographical maps show that the first event after stimulus onset had a maximum activity over occipital electrodes and occurred around 70 ms. The second event presented a strong negative polarity on occipital electrodes with a topography and average time congruent with the N200 (***Nunez et al., 2019***; ***Ritter et al., 1979***). The third and last event precedes the response by a short interval and displays a parietal positivity, congruent with reports of decision-related components following early sensory ones (***Kutas et al., 1977***; ***O'Connell et al., 2012***).

Inter-event times align with encoding and decision laws

If the three detected events capture processes relevant to the decision-making function, we believe that their time of occurrence should be differentially affected by the contrast manipulation. To support this, we fitted Piéron's and Fechner's law as well as a linear model to the inter-event durations, as a function of contrast (***Figure 4*** and ***Table 1***). We found that the first and last intervals

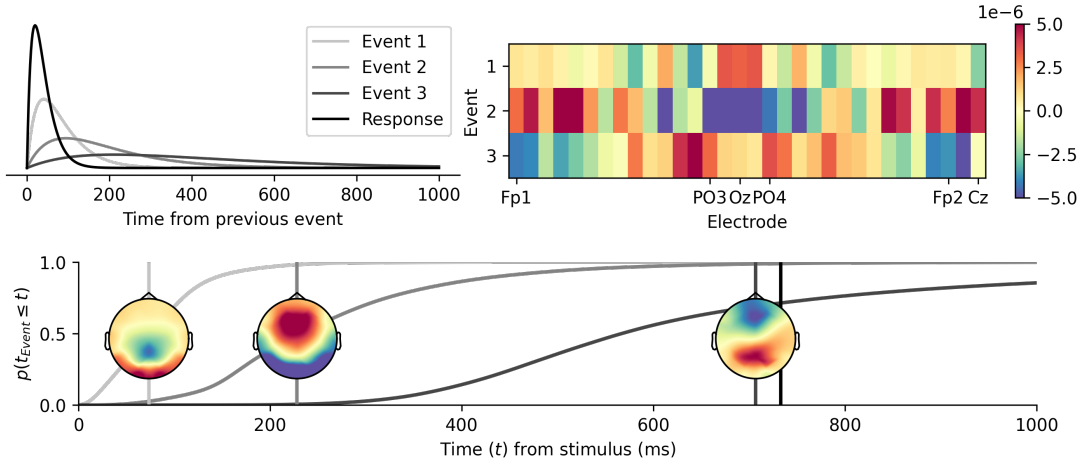

Figure 3. HMP estimation reveals three sequential cognitive events
Top: model components with the inter-event interval distributions estimated for all participants (left) and the weights of each electrode towards each event (right).
Bottom: Trial and participant averaged cumulative event occurrence probabilities for the three detected hidden multivariate events. Overlaid is the average representation of the time location (vertical lines) and electrode contribution of the three identified events based on their by-trial maximum probability.

are best explained by linear models with no relation to the contrast (***Table 2***), but not intervals 2 and 3.

Accuracy	Fechner	Piéron	Linear
Stim.-Resp.	**41.24** ***0.85***	89.93 *0.07*	44.37 *0.83*
Stim.-1	3.51 *0.29*	4.06 *0.06*	**3.43** ***0.33***
1-2	10.64 *-0.05*	**8.84** ***0.25***	9.50 *0.15*
2-3	**39.93** ***0.86***	90.17 *0.09*	44.88 *0.81*
3-Resp.	1.30 *0.03*	1.29 *-0.01*	**1.26** ***0.06***
Speed			
Stim.-Resp.	19.91 *0.27*	23.21 *0.00*	**18.02** ***0.03***
Stim.-1	3.08 *-0.05*	3.20 *-0.05*	**2.78** ***0.19***
1-2	10.31 *0.12*	**6.95** ***0.62***	8.53 *0.43*
2-3	**17.48** ***0.56***	24.73 *0.10*	17.49 *0.57*
3-Resp.	1.09 *0.06*	1.11 *0.02*	**1.05** ***0.09***

Table 1. Square root of the mean prediction error (milliseconds) from the leave-one-out procedure for each interval and model for both instructions (bold indicates the best model). The R^2 (italic) refers to the fit of the predicted *vs.* observed mean durations.

The second interval is best explained by Piéron's law (R^2 Piéron: Speed = 0.62, Accuracy = 0.25, ***Figure 4***, ***Table 1***). The observation that an early interval that seems associated with perception fits Piéron's law is congruent with earlier empirical observations that Piéron's law is associated with stimulus detection (***Piéron, 1913***; ***Banks, 1973***; ***Chocholle, 1940***; ***Overbosch et al., 1989***; ***Bonnet et al., 1999***), contrary to work that argued for a decision-related role (***Stafford and Gurney, 2004***; ***Van Maanen et al., 2012***).

The third interval is best explained by Fechner's law (R^2 Fechner: Speed = 0.56, Accuracy = 0.86). Using the drift rate and decision boundaries estimated from the fit of a Fechner diffusion model (see Methods) on the inter-event durations, we can predict the number of correct responses for each interval. The predictions on the proportion of correct responses further shows that interval 3 predicts the participants' number of correct responses (***Figure 4***) both in accuracy (R^2 = 0.85) and in speed (R^2 = 0.60) while no other interval achieves a comparable fit (all $R^2 < 0$).

These results suggest that in the EEG, two time-periods correspond to stimulus detection and stimulus decision laws, irrespective

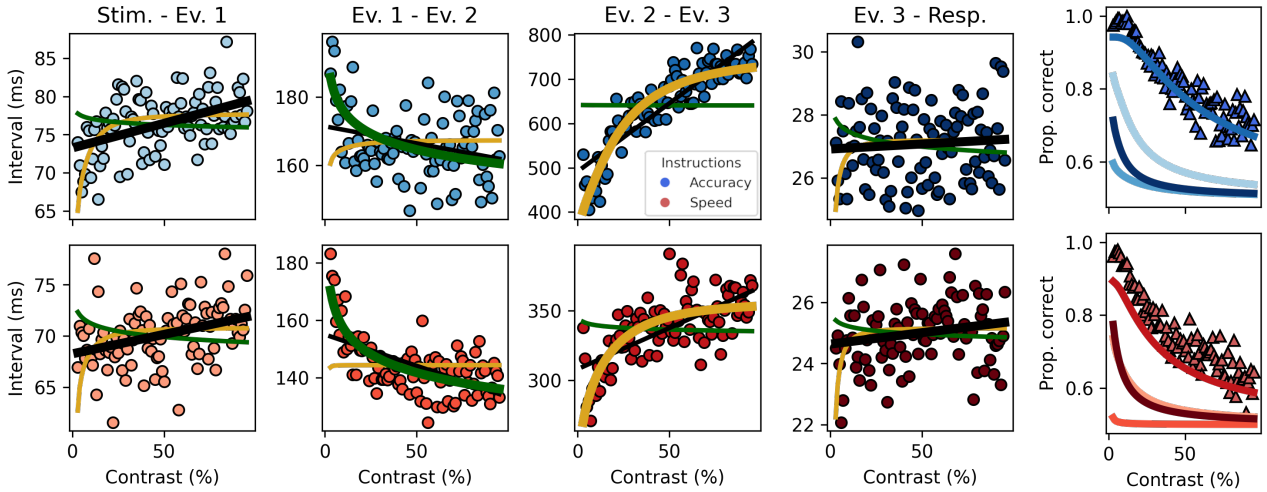

Figure 4. Inter-event interval as a function of experimental factors
The four first panels represent the trial and participant averaged duration between events (stimulus and response respectively as first and last events). The lines represent the fits for the linear (black), Piéron (green) and Fechner (yellow) models. Winning model line is represented as thicker than the other for each panel. The right most panel shows the observed proportion of correct responses (triangles) compared to the prediction (lines) from the Fechner diffusion model fit to each inter-event duration (color saturation indicates order of the interval).

of the speed instructions. To further assess the effect of the experimental factors we used a linear mixed model on the relationship of the timing between events with contrast, SAT and their interaction. Doing so showed that all inter-event durations are sensitive to SAT congruent with previous reports using alternative methodologies and multimodal recording methods or intracranial measurements (***Steinemann et al., 2018***; ***Weindel et al., 2021***; ***Heitz and Schall, 2012***). Congruently with the model selection test, the linear mixed models revealed that only interval 2 and interval 3 display evidence towards an effect of contrast (see ***Table 2*** for effect report). As expected, the duration of the earlier interval 2 presents a negative relationship with contrast (slope = -22ms, CrI = [-30, -15]) while the later interval 3 presents a positive relationship (slope = 59ms, CrI = [23, 101]).

	Intercept	Contrast	SAT	SAT × Cont.
Stim.-1	68.30 (64.48, 71.80)	3.76 (-0.42, 7.97)	5.03 (2.91,7.51)	2.62 (-0.80, 6.17)
1-2	155.03 (146.55, 164.46)	-21.75 (-29.66, -14.03)	16.24 (10.02, 23.69)	11.88 (0.82, 21.33)
2-3	307.60 (269.48, 343.66)	59.34 (23.02, 97.07)	182.57 (128.02, 236.52)	248.71 (156.52, 342.50)
3-Resp.	24.66 (23.62, 25.64)	0.73 (-0.24, 1.68)	2.26 (1.10, 3.32)	-0.39 (-1.64, 1.038)

Table 2. Summary of the linear mixed models coefficients with the maximum a posteriori and the 95% credible intervals in parentheses for the linear mixed models on intervals (top) and electrode match (bottom) for each event (Ev.).

Decision EEG signature occurs as a short-lived pulse before the response

The interval from the second event up to the third event increases with contrast, conforms to Fechner's law and predicts the observed proportion of correct responses. The topography of the third event also supports it being linked to decision processes, as the electrode activity develops as ex-

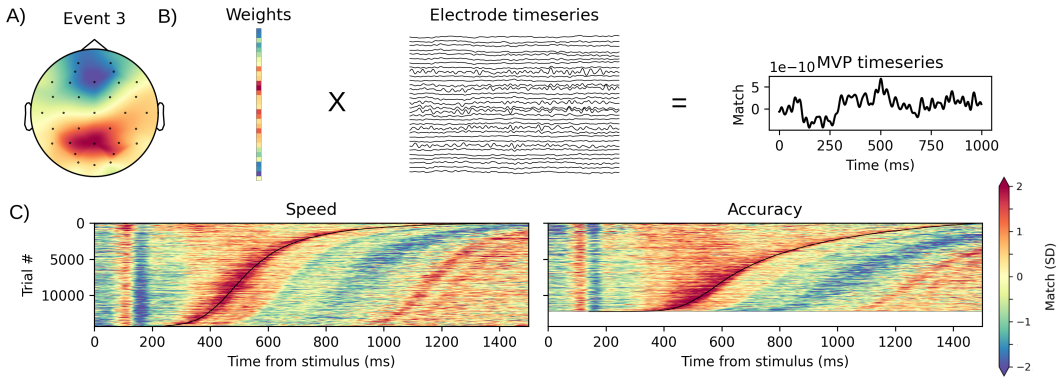

Figure 5. Single trial surface plot of the decision related event
A) Topographical map of the last event, based on the electrode activity at the by-trial most likely time of the event, averaged over trials and participants. B) Spatial filtering using the last event obtained by the dot product between electrode weights of the last event in A) with the single-trial activity of each electrode at all time points resulting in the match between the event topography and the signal (see example timeseries for the first trial of the first participant). C) Surface plot of the match for all trials for speed and accuracy instructions. Zscoring was performed after applying a Gaussian window over 50 trials and with a standard deviation of 20.

pected for decisional processes with a decrease of activation when contrast (and thus difficulty) increases. Therefore, based on its order in the sequence, topography and latency, the last identified EEG event (***Figure 5***A) is the only event displaying decision-related effects. We can track how this decision variable evolves over time by using its topography as a spatial filter and inspecting the time-courses on different reference points in time during the stimulus-response interval. To achieve this we computed the dot product of the electrode weights of that event with the electrode signal at all time steps (***Figure 5***B). This results in single-trial timeseries of the match between the EEG signal and that event's topography (e.g. right panel of ***Figure 5***B). ***Figure 5***C illustrates the single-trial timeseries of the multivariate pattern from stimulus onset, with trials sorted according to the RT, and clearly shows that the last event peaks shortly before the RT (black line in ***Figure 5***C).

A comprehensive analysis of contrast effect on electrophysiological components

So far we have shown that our contrast manipulation impacted the times between the identified EEG events (***Figure 4*** and ***Table 1***) and that we can use the averaged activity at each events' time as spatial filter to build single-trial timeseries (***Figure 5***). Based on the congruence of our results for the three HMP event with previously identified event-related potentials (ERPs) we refer to these events respectively as P100, N200 and centro-parietal positivity (CPP).

To test how the EEG activity leading up to each of these components is affected by the contrast manipulation, we computed the single-trial timeseries for each event as in ***Figure 5***. We centered all trials based on the most-likely time of the peak of each event and tested if the period preceding each event up to the previous one was sensitive to the contrast manipulation by performing a non-parametric cluster-level paired t-test for the participant averaged time-series for low (< 50%) *vs.* high (> 50%) contrasts (***Figure 6***).

For the period between the stimulus onset and the peak of the P100 (***Figure 6***, left panel), this analysis show that the single-trial timeseries of the P100 are impacted by contrast around the detected event, with lower contrasts yielding lower activation of the event. The N200 however (***Figure 6***, middle panel) does not show a period of significant contrast effect in the direct vicinity of the N200. A period of significant difference is however present in an interval between 50 and 125ms before the N200. This indicates that a component, with a topography opposite to the N200 (given the sign of the match with the topography), is impacted by the contrast manipulation in the same direction as the P100. For the last detected event (the CPP, ***Figure 6***, right panel), a significant

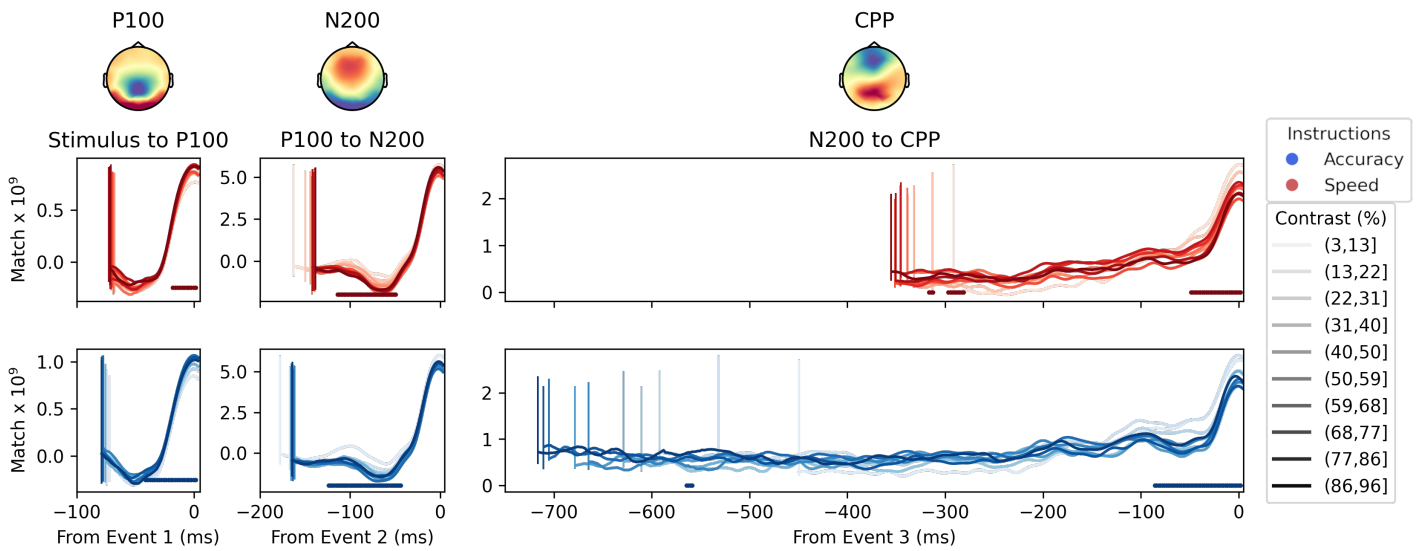

Figure 6. Electrophysiological analysis of the time leading to each event
For each HMP detected event we used the average topographies (top panel) as a spatial filter for the samples from the by-trial event peak time down to the average time of the previous event (vertical lines). For each speed and accuracy instructions, all trials were averaged across 10 bins of contrast values. To statistically test for an effect of contrast we performed a non-parametric cluster-level paired t-test for high (> 50%) vs. low (< 50%) contrasts. Significant clusters are marked as dots in the lower part of each panel.

period of difference between high and low contrasts occurs at the peak of the event which lasts for a time up to 50 to 100ms before the peak of the CPP. The duration of this period appears shorter in the speed condition than in the accuracy condition. This is congruent with an account of a centro-parietal positivity building up as a ramp before the decision commitment (***O'Connell et al., 2012***). To further test how this electrophysiological development relate to behavior we inspected the relation between this build-up and behavior in ***Box 1***.

Discussion

By modeling the recorded EEG signal between stimulus onset and response as a sequence of by-trial recurrent topographical events with varying by-trial peak times, we detected three events in the RT of participants performing a simple visual decision-making task. To identify specific cognitive processes, we combined this approach with a targeted manipulation of stimulus intensity expected to elicit two well-known psychophysical laws relating to stimulus encoding and decision, respectively Piéron's and Fechner's laws. Relating inter-event intervals and electrode activity to these laws allowed us to unambiguously map the expected cognitive processing steps to the three events discovered in the single-trial EEG between the stimulus onset and the production of a response.

The first event after stimulus onset most likely represents early visual processing; the expression of this P100 component in the EEG is changed by the contrast of the stimulus in the direction expected for visual processing (***Figure 6***). However, we did not find evidence for a modulation of its peak time (***Figure 4***) dependent on contrast, likely because its onset is triggered by a visible cue indicating trial start. After this P100 and a duration influenced by the stimulus contrast according to Piéron's law (***Figure 4***), the second event peaks with an overall timing and topography that resembles the N200 (***Figure 3***), a component linked to figure-ground separation (***Ritter et al., 1979***). It is interesting to note that, while this N200 peak time respective to the P100 is linked to visual processing, we did not find evidence for visual or decision related effects in the EEG expression of that event (***Figure 6***). We thus conclude that the second event represents the attention orientation process whose timing predicts the decision-making onset, congruent with previous findings

Box 1. Predicting decision-making behavior from the CPP build-up

The idea of electrophysiological signals reflecting evidence accumulation has received critical considerations (***Latimer et al., 2015***; ***Frömer et al., 2024***; ***Zoltowski et al., 2019***). Using the isolated decision-related event identified in this study, we can assess to what extent the signal before the last detected event – which we linked to the decision – resembles an evidence accumulation ramp (***O'Connell et al., 2012***). To study this, we computed the match between the decision topography in ***Figure 5***A and the samples in between the by-trial estimated peak of the event and the 250ms period preceding it (defined based on the minimum average decision time in ***Figure 4***). We then performed a linear regression for each participant and each contrast level.

Firstly, using a one-sample, one-sided, t-test, we observed that the distribution of the slopes for all contrast-levels, averaged over participants, were significantly higher than 0 both in speed ($t(92) = 31.95, p < 0.0001$) and accuracy ($t(92) = 21.11, p < 0.0001$). Secondly, we computed the Pearson correlation coefficient between the contrast averaged proportion of correct responses and either the intercepts or slopes of the linear regression models, averaged over participants, for each contrast level. Our reasoning was that, if a ramp is present in the build-up of the decision relevant event, and if this ramp is related to the difficulty of the decision, then the slope of the linear regression models should correlate with the proportion of correct responses of the participants. The intercepts of the regression models, in turn, should represent the amount of evidence that is accumulated (represented by the value of the component at decision commitment).

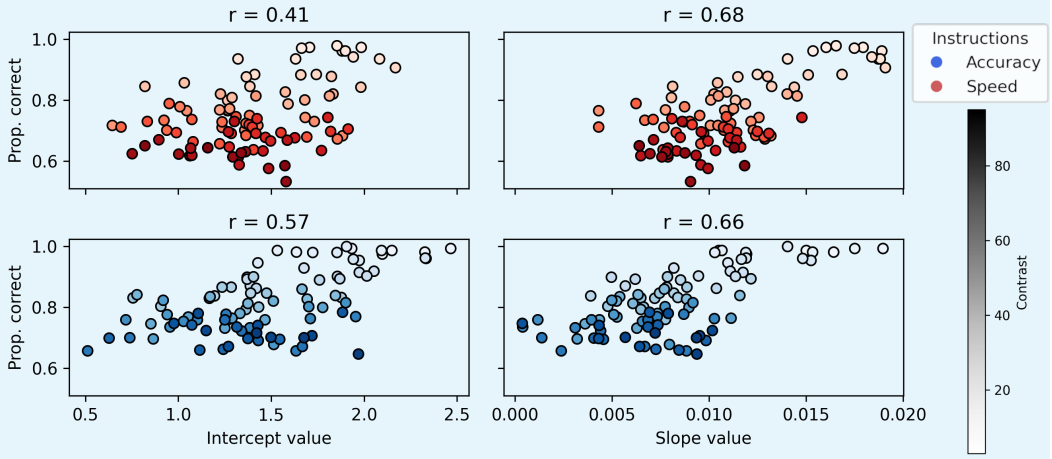

As can be seen in the Figure, both the intercepts and slopes of the linear models predict the proportion of correct responses with correlation coefficient ranging from 0.41 to 0.68 (all p-values < 0.0001). These observations support the hypothesis that a ramping signal, congruent with evidence accumulation, is developing prior to the response of the participants. Furthermore, assuming that the intercept of the linear regression models accurately reflect the value of evidence at choice commitment, the observation that the intercept predicts the proportion of correct response supports a decision-making model with a decision threshold dynamically decreasing over time (***Drugowitsch et al., 2012***; ***Tajima et al., 2016***; ***Van Maanen et al., 2016***). This is because under the assumption of a decreasing threshold, a lower rate of evidence accumulation will cross the decision threshold at a lower value, here represented by a smaller intercept.

(***Nunez et al., 2019***). Finally, the last event terminates the decision as shown by the observation that the time from the attention orientation peak to this last event peak is best fitted by a Fechner diffusion model and that the estimated parameters predict the proportion of correct responses at a high accuracy ($R^2 \geq 0.6$). In light of previously identified EEG components it can come as a surprise that no event presents a lateralization congruent with the side of the response. The absence of such lateralized readiness potentials (***Coles et al., 1985***) in the present study could be linked to the fact that we minimized motor engagement by asking participants to always provide a response with the right hand by using either their index or middle finger to answer respectively left or right on a standard keyboard. Alternatively, it might also be related to the fact that the start of response execution does not sign the end of a decision (***Weindel, 2021***) and thus that the time of response execution is less predictive of the RT (***Weindel et al., 2021***).

Therefore, to the question of the processing steps in the RT raised by Franciscus C. Donders (***Donders, 1868***) and Hermann von Helmholtz (***von Helmholtz, 2021***) more than a century ago, we can affirm that the RT in this decision-making task is made up of three steps: visual encoding, attention orientation and decision-making. This decomposition of the RT into processing steps allows to explicitly test the impact of experimental conditions, inter-individual factors, or different strategies (***Den Otter et al., 2025***). Furthermore, the by-trial resolution allows to use the extracted times to address what theory best explains observed behavior (***Turner et al., 2017***; ***Ghaderi-Kangavari et al., 2022***) as shown by our ability to fit evidence accumulation on the estimated inter-event durations. This likely represents a critical step for a modern approach to mental chronometry in which the analysis of neural data is constrained by the behavior and in turns informs on the generative model of behavior (***Meyer et al., 1988***).

Accessing the most likely time of task relevant EEG components further allows to apply advanced signal analysis methods. In this study, instead of picking electrodes based on a priori hypotheses and analyzing their activity, we used the average topographies obtained by averaging electrode activity at the most-likely time of the event at each trial. Doing so allowed us to use these topographies as spatial filters to analyze the expression of that topography in the vicinity of the events' time location. This made it possible to provide support for the idea that the EEG signal preceding the response is made of a ramp that evolves congruently with the decision being made. Other work with different methods or species (***Latimer et al., 2015***; ***Frömer et al., 2024***; ***Zoltowski et al., 2019***) have instead found support for a discrete event linked to the response. The ERPs on the by-trial centered event in ***Figure 6*** show support for both accounts. The main component of the CPP ERP is the short burst-like activity whose by-trial amplitude varies with decisional difficulty. Nevertheless, the build-up of the decisional signal between high vs low contrast diverges earlier than the 50ms expected pattern. Furthermore ***Box 1*** shows that both the intercept (value at the events' peak) and the slope (build-up of the signal) of a linear regression model fitted on the spatially filtered samples between the events peak and the activity prior to the peak, predict participants accuracies. This means that rate of build-up of the decisional event as well as the value before the response contain information on the likelihood of the participant making a correct response. Finally, simulating EEG data with a ramping function, as expected from evidence accumulation models, shows that the ERP profile for such a simulation (Appendix 1) is again compatible with two components of decisions. In this simulation, on one hand the simulated ERP shows a similar build-up as the real one ***Figure 6***, and on the other hand no pulse-like activity is found, showing that simulating a ramp is not enough to account for the observed ERP. Thus, as proposed using intracranial recordings in monkeys (***Stine et al., 2023***), we concur that decision-related signals can be best explained by both a progressive accumulation predicting correctness and a decision termination event whose timing and activity represent the crossing of a decision threshold (***Box 1***).

Conclusion

Overall, this study adds to the growing body of research that suggests that electrophysiological signals co-registered during behavior can be decomposed into discrete neural events whose rel-

ative timing is informative on the computation performed by the brain (***Berberyan et al., 2021***; ***Zhang et al., 2018***; ***Anderson et al., 2016***, ***2018***; ***Krause et al., 2024***; ***Van Maanen et al., 2021***; ***Weindel et al., 2021***). In the case of decision-making these discrete neural events are visual encoding, attention-orientation and decision commitment and their latency make up the reaction time.

Materials and Methods

Participants

26 participants with normal or corrected-to-normal vision and no history of neurological diseases signed an informed consent form to participate in the study. The study was validated by the CETO ethical committee of the University of Groningen (ID 94056673). All participants received a compensation of 12EUR for a session of 90 minutes including EEG set-up.

Task

The participants performed the experiment in a shielded window-less EEG Lab. They were seated approximately 90 cm from a 24-inch LCD screen with a refresh rate of 60 Hz. Participants indicated their response used index and middle finger of their right hand on the "n" and "m" keys respectively for left and right responses. The inter-trial interval from the response to trial n to the stimulus of trial $n+1$ was randomly sampled from a uniform distribution between 0.5 and 1.25 seconds. Self-paced breaks were interspersed every 140 trials. Participants were instructed to keep their gaze on the fixation cross during the blocks of trials. Speed and accuracy feedback was provided at the end of each block with eventual oral feedback in case the responses were not fast or accurate depending on the SAT instruction. The SAT instructions were displayed at the beginning of each block and varied every two blocks of trials. Participants were trained on the task and on the SAT instructions for 10 minutes with a short block of alternating SAT instructions with corresponding feedback.

Stimuli were controlled by the *psychopy* python package (***Peirce, 2007***). The stimuli consisted of two sinusoidal gratings on the left and right of a fixation cross. The gratings had a size of 2.5 degrees of visual angle and a horizontal spatial frequency of 1.2. The contrast was manipulated by setting a contrast value for both gratings and subtracting 2.5% contrast on the incorrect side and adding 2.5% on the correct side. For each trial the initial contrast was sampled from a uniform distribution with a minimum of 3.5% contrast to a maximum of 95.5% of contrast. Timing of the stimulus was corrected based on a photodiode.

EEG

EEG data were acquired from 32 electrodes using a BioSemi Active Two system at a sampling rate of 1024Hz. Additionally, two electrodes were placed at each outer canthus and one below the left eye to record horizontal and vertical (by combining with Fp1) electro-oculograph. Two electrodes were placed on the mastoid bones for reference during acquisition only and for inspection of bad electrodes. For most of the participants, scalp impedance of the electrodes was kept at $< 20k\Omega$, except for two participants where it was kept at $< 30k\Omega$. The data was recorded using the BioSemi acquisition program ActiView 811.

All preprocessing was done using the *mne* package (v1.9.0) (***Gramfort et al., 2014***) with a semi-automated preprocessing custom script (see the Github repository). First, a template montage for the EEG electrode positions was applied, the signal was visually inspected for bad electrodes (9 in total for the 26 participants). The trigger indicating the time of stimulus onset was corrected based on the signal of a co-registered photodiode. The signal was then low-pass filtered at 40 Hz (to avoid rejection by μV threshold of high frequency activity, see next section) and re-referenced to the average of the electrodes. An ICA was performed to remove ocular related activity on a 256 Hz downsampled version, bandpass filtered between 1 and 80 Hz and epoched based on stimulus onsets. The independent component rejection was partially automated by using the correlation of the IC timecourse to the vertical and horizontal EOG. Visual inspection of the independent components was used to ensure a proper classification. On average 1.88 components were removed (max = 3). The rejected ICs were zeroed out on the low-pass filtered signal and (eventual) bad electrodes were then interpolated using spherical splines. The epochs were then created by using 200 ms before the stimulus as baseline correction and keeping samples up to 3000ms after stimulus.

Analyses

Trials in which an electrode exceeded 100 μV between stimulus and response were discarded. Trials with an RT shorter than 100 ms, or exceeding the epoching window of 3 seconds were discarded. Overall, 6.3% of the recorded trials were rejected for all the analyses presented in the paper. All analyses were performed using python (v3.12.3). All RTs were given an offset of 10 ms to avoid edge effects in the cross-correlation involved by HMP.

Hidden multivariate pattern

The HMP analyses followed the pipeline suggested in (***Weindel et al., 2024***) and applied using the *hmp* package (v1.0.0-b.1) . The EEG data was first truncated to the data between stimulus onset and response. A PCA was applied to the average of the participant variance-covariance matrices. The 15 first principal components (PCs), explaining more than 99.9% of the variance, were retained. The resulting time-series were z-scored per-participant by subtracting the participant mean and dividing by the participant standard deviation for each trials of all combined PCs. The resulting dataset was used in the HMP estimation. The HMP model was fitted with the expectation of a 50 ms event duration as used in previous applications. The number of events was estimated using the standard cumulative fit routine with the default parameters of the associated python package. We fitted the same model to the data of all participants across all conditions.

Linear mixed models

The (General) linear mixed models included SAT instructions, contrast and their interaction as predictor and the maximum random effect structure given the fixed effects formulation. Predictors were coded with SAT predictor as treatment contrasted with speed as 0 and accuracy as 1, contrast was treated as numerical from 0 to 1. The general linear mixed model on proportion of correct responses was performed using a logit link. The linear mixed models were performed on the raw milliseconds scale for the interval durations and on the standardized values for the electrode match. To ensure convergence the models were fitted using a Bayesian estimation with 4 MCMC chains, and 2000 samples (1000 as tuning samples) using the bambi Python package (v0.15.0) (***Capretto et al., 2022***) with default priors weakly informed by the data. Posterior distribution were summarized with the point estimate of the maximum a posteriori and 95% credible interval (CrI) computed with the Arviz Python package (v0.21.0) (***Kumar et al., 2019***) based on the highest density interval (***Kruschke, 2010***).

Permutation cluster analysis

To test the significance of the time steps in the ERP analyses we first computed the timeseries of each event (as illustrated in ***Figure 5***) for all trials from the peak of the event up to the average peak time of the preceding event (stimulus being the first event). For convenience in the use of the statistical test, the contrast conditions were splitted to aggregate values lower and higher than 50%. To control for the multiple comparison involved by the significance test at each time-point we used a non-parametric cluster-level paired t-test as implemented in the *mne* package (***Gramfort et al., 2014***) using the default values (version 1.8.0). Rejecting the null hypothesis indicates that the cluster structure in each condition (here low vs high contrast) is not exchangeable (***Sassenhagen and Draschkow, 2019***).

Model fits

Piéron's law (***Piéron, 1913***) predicts that the time to perceive (T_P) will be negatively related to the contrast (C) values (***Figure 1***):

$$T_P = \beta C^{-\alpha} \tag{1}$$

With a modality/individual specific adjustment slope (β) and exponent (α). In contradistinction, Fechner's law (***Fechner, 1860***) states that the perceived difference (p) between the two patches fol-

lows the logarithm of the difference in physical intensity between the contrasts of the two patches:

$$p = \beta \log \frac{C_1}{C_0} \tag{2}$$

Again with a modality and individual specific adjustment slope (β). By connecting this perceived difference to a decision model with an accumulation to bound mechanism (***Palmer et al., 2005***) we can predict the mean RT for a set of stimuli and three estimated parameters: the adjustment β, a decision criterion (A) and a residual time (T_0):

$$RT = \frac{A}{\beta p}\tanh(A\beta p) + T_0 \tag{3}$$

Where a difference (δ, 0.05 in the current experiment) result in a perceived difference (p) given by Fechner's law:

$$p = \log(\frac{C + \delta/2}{C - \delta/2}) \tag{4}$$

This model then states that the decision easiness (i.e. drift rate, βp) is determined by the perceived difference between two stimuli p. The proportion of correct responses (P_C), given the definition of the proportional rate diffusion model(***Palmer et al., 2005***) is then given by:

$$P_c = \frac{1}{1 + e^{-2A\beta p}} \tag{5}$$

The model thus predicts that, for a constant physical difference δ between stimulus, the RT will increase with the overall contrast values (***Figure 1***) while the likelihood of being correct will decrease.

All these models were fitted per participant using the trust region reflective algorithm implemented in *scipy* (v1.15.2) (***Virtanen et al., 2020***). Models were fitted individually, predictions presented in the paper were aggregated across individual predictions. The estimation of the exponent and slope of Piéron's law were constrained to be negative according to the theoretical formulation. The Fechner diffusion model was constrained based on the parameters observed for similar models (***Tran et al., 2021***). The cross-validation was performed by estimating the models with one contrast value left-out, and evaluated by computing the rootsquare of the mean-squared prediction error between the left-out contrast and the predictions of the model.

Data and code availability

The data and code associated with this manuscript can be found on the associated OSF and Github repositories.

Acknowledgements

We thank Kenneth Müller for his help in coding the task and collecting the data and Samson Chota for his suggestions on the analyses presented in the paper. We thank Leon Kenemans, Chris Klink, Ben Harvey and Michael Nunez for the discussion on the present findings. Finally, GW wishes to thank Anna Montagnini and Frédéric Chavane for the informal discussion that ultimately lead to this paper. No AI-assisted technologies was used to write the paper or the associated code.

Funding

This project has received funding from the European Union's Horizon 2020 research and innovation programme under the Marie Skłodowska-Curie grant agreement No 101066503. JPB and LvM are funded through the Air Force Research Laboratory grant No EOARD FA8655-22-1-7003.

References

Anderson JR, Borst JP, Fincham JM, Ghuman AS, Tenison C, Zhang Q. The common time course of memory processes revealed. Psychological science. 2018; 29(9):1463–1474.

Anderson JR, Zhang Q, Borst JP, Walsh MM. The discovery of processing stages: Extension of Sternberg's method. Psychological review. 2016; 123(5):481.

Banks WP. Reaction time as a measure of summation of warmth. Perception & Psychophysics. 1973; 13:321–327.

Başar E. EEG-brain dynamics: relation between EEG and brain evoked potentials Elsevier. North-Holland Biomedical Press; 1980.

Berberyan HS, van Rijn H, Borst JP. Discovering the brain stages of lexical decision: Behavioral effects originate from a single neural decision process. Brain and Cognition. 2021; 153:105786.

Bonnet C, Zamora MC, Buratti F, Guirao M. Group and individual gustatory reaction times and Piéron's law. Physiology & Behavior. 1999; 66:549–558.

Borst JP, Anderson JR. Discovering cognitive stages in M/EEG data to inform cognitive models. In: *An introduction to model-based cognitive neuroscience* Springer; 2024.p. 101–117.

Capretto T, Piho C, Kumar R, Westfall J, Yarkoni T, Martin OA. Bambi: A Simple Interface for Fitting Bayesian Linear Models in Python. Journal of Statistical Software. 2022; 103(15):1–29. doi: 10.18637/jss.v103.i15.

Chocholle R. Variation des temps de réaction auditifs en fonction de l'intensité à diverses fréquences. L'Année Psychologique. 1940; 41:65–124.

Coles MG, Gratton G, Bashore TR, Eriksen CW, Donchin E. A psychophysiological investigation of the continuous flow model of human information processing. Journal of Experimental Psychology: Human Perception and Performance. 1985; 11(5):529.

Den Otter R, Weindel G, Stuit S, van Maanen L. Sequence models for by-trial decoding of cognitive strategies from neural data. arXiv preprint arXiv:250410028. 2025; .

Donders FC. Die schnelligkeit psychischer processe: Erster artikel. Archiv für Anatomie, Physiologie und wissenschaftliche Medicin. 1868; p. 657–681.

Drugowitsch J, Moreno-Bote R, Churchland AK, Shadlen MN, Pouget A. The cost of accumulating evidence in perceptual decision making. Journal of Neuroscience. 2012; 32(11):3612–3628.

Fechner GT. Elemente der psychophysik, vol. 2. Breitkopf u. Härtel; 1860.

Frömer R, Nassar MR, Ehinger BV, Shenhav A. Common neural choice signals can emerge artefactually amid multiple distinct value signals. Nature Human Behaviour. 2024; 8(11):2194–2208.

Ghaderi-Kangavari A, Rad JA, Parand K, Nunez MD. Neuro-cognitive models of single-trial EEG measures describe latent effects of spatial attention during perceptual decision making. Journal of Mathematical Psychology. 2022; 111:102725. https://www.sciencedirect.com/science/article/pii/S0022249622000633, doi: https://doi.org/10.1016/j.jmp.2022.102725.

Gramfort A, Luessi M, Larson E, Engemann DA, Strohmeier D, Brodbeck C, Parkkonen L, Hämäläinen MS. MNE software for processing MEG and EEG data. neuroimage. 2014; 86:446–460.

Heitz RP, Schall JD. Neural mechanisms of speed-accuracy tradeoff. Neuron. 2012; 76(3):616–628.

von Helmholtz H. In: Schmidgen H, editor. Mittheilung für die physikalische Gesellschaft in Berlin betreffend Versuche über die Fortpflanzungsgeschwindigkeit der Reizung in den sensiblen Nerven des Menschen Berlin, Heidelberg: Springer Berlin Heidelberg; 2021. p. 137–139. https://doi.org/10.1007/978-3-662-63833-0_6, doi: 10.1007/978-3-662-63833-0_6.

Kelly SP, Corbett EA, O'Connell RG. Neurocomputational mechanisms of prior-informed perceptual decision-making in humans. Nature Human Behaviour. 2021; 5(4):467–481.

Krause J, van Rij J, Borst JP. Word type and frequency effects on lexical decisions are process-dependent and start early. Journal of Cognitive Neuroscience. 2024; 36(10):2227–2250.

Kruschke JK. Bayesian data analysis. Wiley Interdisciplinary Reviews: Cognitive Science. 2010; 1(5):658–676.

Kumar R, Carroll C, Hartikainen A, Martin O. ArviZ a unified library for exploratory analysis of Bayesian models in Python. Journal of Open Source Software. 2019; 4(33):1143. https://doi.org/10.21105/joss.01143, doi: 10.21105/joss.01143.

Kutas M, McCarthy G, Donchin E. Augmenting mental chronometry: the P300 as a measure of stimulus evaluation time. Science. 1977; 197(4305):792–795.

Latimer KW, Yates JL, Meister ML, Huk AC, Pillow JW. Single-trial spike trains in parietal cortex reveal discrete steps during decision-making. Science. 2015; 349(6244):184–187.

Luce R. Response Times: Their Role in Inferring Elementary Mental Organization. Oxford University Press New York; 1986. doi: 10.1093/acprof:oso/9780195070019.001.0001.

Luck SJ. Ten simple rules for designing and interpreting ERP experiments. Event-related potentials: A methods handbook. 2005; 4.

Makeig S. Response: event-related brain dynamics–unifying brain electrophysiology. Trends in neurosciences. 2002; 25(8):390.

Meyer DE, Osman AM, Irwin DE, Yantis S. Modern mental chronometry. Biological Psychology. 1988; 26(1-3):3–67.

Nunez MD, Gosai A, Vandekerckhove J, Srinivasan R. The latency of a visual evoked potential tracks the onset of decision making. Neuroimage. 2019; 197:93–108.

O'Connell RG, Corbett EA, Pares-Pujolras E, Feuerriegel D, Kelly SP. Regressing Away Common Neural Choice Signals does not make them Artifacts. Comment on Fromer et al (2024, Nature Human Behaviour). bioRxiv. 2024; p. 2024–09.

O'Connell RG, Dockree PM, Kelly SP. A supramodal accumulation-to-bound signal that determines perceptual decisions in humans. Nature neuroscience. 2012; 15(12):1729–1735.

Overbosch P, de Wijk R, de Jonge TJ, Köster EP. Temporal integration and reaction times in human smell. Physiology & Behavior. 1989; 45:615–626.

Palmer J, Huk AC, Shadlen MN. The effect of stimulus strength on the speed and accuracy of a perceptual decision. Journal of vision. 2005; 5(5):1–1.

Peirce JW. PsychoPy—psychophysics software in Python. Journal of neuroscience methods. 2007; 162(1-2):8–13.

Piéron H. II. Recherches sur les lois de variation des temps de latence sensorielle en fonction des intensités excitatrices. L'année psychologique. 1913; 20(1):17–96.

Ratcliff R, McKoon G. The diffusion decision model: theory and data for two-choice decision tasks. Neural computation. 2008; 20(4):873–922.

Ritter W, Simson R, Vaughan Jr HG, Friedman D. A brain event related to the making of a sensory discrimination. Science. 1979; 203(4387):1358–1361.

Sassenhagen J, Draschkow D. Cluster-based permutation tests of MEG/EEG data do not establish significance of effect latency or location. Psychophysiology. 2019; 56(6):e13335.

Schurger A, Sitt JD, Dehaene S. An accumulator model for spontaneous neural activity prior to self-initiated movement. Proceedings of the National Academy of Sciences. 2012; 109(42):E2904–E2913.

Shadlen MN, Kiani R, Newsome WT, Gold JI, Wolpert DM, Zylberberg A, Ditterich J, de Lafuente V, Yang T, Roitman J. Comment on "Single-trial spike trains in parietal cortex reveal discrete steps during decision-making". Science. 2016; 351(6280):1406–1406. https://www.science.org/doi/abs/10.1126/science.aad3242, doi: 10.1126/science.aad3242.

Smyrnis N, Mylonas DS, Rezaie R, Siettos CI, Ventouras E, Ktonas PY, Evdokimidis I, Papanicolaou AC. Single-trial magnetoencephalography signals encoded as an unfolding decision process. Neuroimage. 2012; 59(4):3604–3610.

Stafford T, Gurney KN. The role of response mechanisms in determining reaction time performance: Piéron's law revisited. Psychonomic Bulletin & Review. 2004; 11:975–987.

Steinemann N, Stine GM, Trautmann E, Zylberberg A, Wolpert DM, Shadlen MN. Direct observation of the neural computations underlying a single decision. Elife. 2024; 12:RP90859.

Steinemann NA, O'Connell RG, Kelly SP. Decisions are expedited through multiple neural adjustments spanning the sensorimotor hierarchy. Nature communications. 2018; 9(1):3627.

Stine GM, Trautmann EM, Jeurissen D, Shadlen MN. A neural mechanism for terminating decisions. Neuron. 2023; 111(16):2601–2613.

Tajima S, Drugowitsch J, Pouget A. Optimal policy for value-based decision-making. Nature communications. 2016; 7(1):12400.

Tran NH, Van Maanen L, Heathcote A, Matzke D. Systematic parameter reviews in cognitive modeling: Towards a robust and cumulative characterization of psychological processes in the diffusion decision model. Frontiers in psychology. 2021; 11:608287.

Turner BM, Forstmann BU, Love BC, Palmeri TJ, Van Maanen L. Approaches to analysis in model-based cognitive neuroscience. Journal of Mathematical Psychology. 2017; 76:65–79.

Van Maanen L, Fontanesi L, Hawkins GE, Forstmann BU. Striatal activation reflects urgency in perceptual decision making. NeuroImage. 2016; 139:294–303.

Van Maanen L, Grasman RPPP, Forstmann BU, Wagenmakers EJ. Piéron's law and optimal behavior in perceptual decision-making. Frontiers in Decision Neuroscience. 2012; 5:article 143.

Van Maanen L, Portoles O, Borst JP. The discovery and interpretation of evidence accumulation stages. Computational brain & behavior. 2021; 4(4):395–415.

Vidaurre D, Myers NE, Stokes M, Nobre AC, Woolrich MW. Temporally unconstrained decoding reveals consistent but time-varying stages of stimulus processing. Cerebral Cortex. 2019; 29(2):863–874.

Virtanen P, Gommers R, Oliphant TE, Haberland M, Reddy T, Cournapeau D, Burovski E, Peterson P, Weckesser W, Bright J, van der Walt SJ, Brett M, Wilson J, Millman KJ, Mayorov N, Nelson ARJ, Jones E, Kern R, Larson E, Carey CJ, et al. SciPy 1.0: Fundamental Algorithms for Scientific Computing in Python. Nature Methods. 2020; 17:261–272. doi: 10.1038/s41592-019-0686-2.

Weindel G. On the measurement and estimation of cognitive processes with electrophysiological recordings and reaction time modeling. PhD thesis, Aix-Marseille; 2021.

Weindel G, Anders R, Alario F, Burle B. Assessing model-based inferences in decision making with single-trial response time decomposition. Journal of Experimental Psychology: General. 2021; 150(8):1528.

Weindel G, van Maanen L, Borst JP. Trial-by-trial detection of cognitive events in neural time-series. Imaging Neuroscience. 2024; 2:1–28.

Woldorff MG. Distortion of ERP averages due to overlap from temporally adjacent ERPs: Analysis and correction. Psychophysiology. 1993; 30(1):98–119.

Zhang Q, Van Vugt M, Borst JP, Anderson JR. Mapping Working Memory Retrieval in Space and in Time: A Combined Electroencephalography and Electrocorticography Approach. NeuroImage. 2018 Jul; 174:472–484. doi: 10.1016/j.neuroimage.2018.03.039.

Zoltowski DM, Latimer KW, Yates JL, Huk AC, Pillow JW. Discrete stepping and nonlinear ramping dynamics underlie spiking responses of LIP neurons during decision-making. Neuron. 2019; 102(6):1249–1258.

Zylberberg A, Dehaene S, Roelfsema PR, Sigman M. The human Turing machine: a neural framework for mental programs. Trends in cognitive sciences. 2011; 15(7):293–300.

Appendix 1

Assuming half-sines when the signal is a ramp

Based on two theories of ERP generation (***Makeig, 2002***; ***Başar, 1980***), the HMP method assumes that searching for multivariate half-sines in the EEG signal is relevant to capture significant changes in cognitive processing. Theories aside, given the oscillatory nature of EEG signals, the use of a half-sine pattern can also be seen as the most entropic pattern to capture a wide range of EEG signals. In the case of the CPP, it is believed that this potential arises from ramping activity at the single-trial level. The main text suggests that this ramping activity is present and thus that the method used is able to capture such an activity. Nevertheless, to formally test whether HMP could also detect an event if it was comprised of a ramp like signal, we simulated data congruent with this hypothesis.

We first downsampled the signal to 100Hz for computational reasons and re-estimated an HMP model as in the main results. We used the downsampled data structure without any real data and added, at the by-trial most-likely times, the pattern of each event. To add the pattern to the 0 signal we computed the outer product between the patterns activation and the values of the electrodes at the most likely time of each event by-trial. The two first events were simulated as half-sines: the activation pattern was defined as the first 5 samples of a full 10Hz sine-wave sampled at 100Hz (i.e. 50ms pulse like activity). The last event was simulated as an accumulation trace. This was achieved by generating 100,000 cumulative sums of Gaussian noise with both mean and standard deviation set to 0.1 over 2000 time steps. These cumulative sums form simulated accumulation traces. For each simulated accumulation trace we recorded the time step at which a decision threshold was crossed by monitoring the first time the absolute cumulative sum exceeded the value 1 (traces that reached a threshold of -1 were inverted). For each simulated trial, to avoid a too high impact of noise, we averaged the 10 traces with the closest time to the actual time between the 2nd event and the response. The pattern was then added between the 2nd event and the response. After having imputed the three patterns to each trial at their corresponding times, we added noise based on the variance-covariance matrix between electrodes observed in the real data, computed during the 200ms baseline of the epochs, using a multivariate normal and an infinite impulse response filter (with 0.2, -0.2 and 0.04 as denominator coefficients as done in ***Weindel et al., 2024***) as implemented in *scipy* (v1.15.2) (***Virtanen et al., 2020***). We then estimated an HMP model as in the main text and described in the method section, using the standard assumption of a 50ms half-sine or pulse-like activity.

As can be seen in the top panel of Figure 1 of this Appendix, despite the generating signal not being the half-sine pattern expected by HMP, the model still finds evidence for three events with the same average topographies and times as estimated on the real data (***Figure 3***). This happens because the accumulation trace in the simulated data increases the cross-correlation of the signal with a half-sine. Because this increased cross-correlation is repeated across trials and followed by the response, it allows the model to detect the event. However, this activity seems to make the detection of the other events less clear than in the real data (based on the comparison with the amplitudes of ***Figure 3***) On the EEG expression of the decision-related event, it can be seen in the middle and lower panels of Figure 1 that, even though the model assumes a different pattern, the ERP from the third detected event, created using the topography of the third event as spatial filter (as in ***Figure 6***), shows a progressive ramp evolving as expected with decision difficulty (contrast), leading to comparable significance patterns for low vs high contrasts (see Methods and ***Figure 6***). However, contrary to the real data we do not observe a burst at the event's most

likely time, showing that the pulse-like activity in ***Figure 6*** is a consequence of the data and not the assumption of the HMP method.

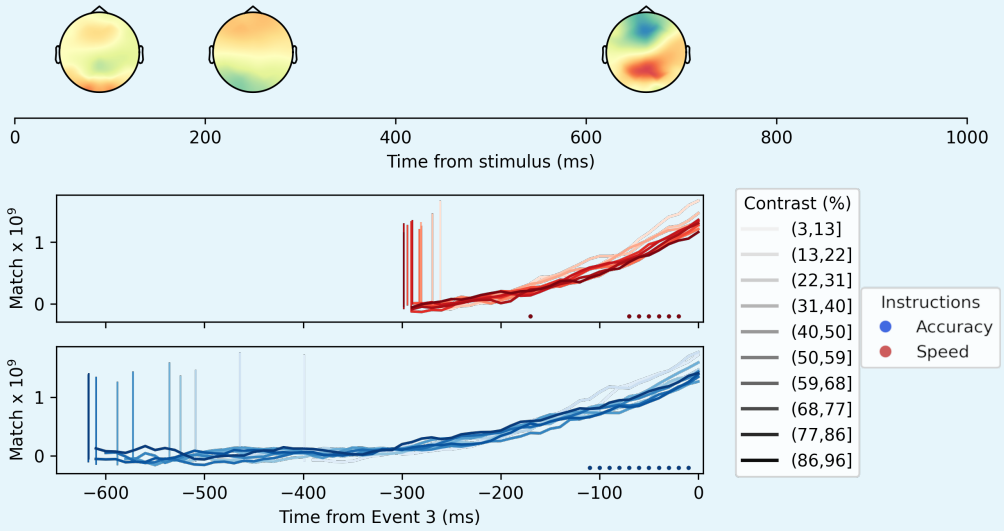

Figure 1. Simulating ramp and expecting a half-sine
Top: Representation of the averaged times and topographies for the three events detected by HMP on the simulated accumulation data. Bottom: Trial and participant averaged time-course of the electrodes matched to the third HMP event. The trials were first centered on the peak of the third event before computing the average ERP for the different contrast values binned into 10 bins. Dots indicate significant differences between high (> 50%) and low (< 50%) contrast values.